Inversion of SV-to-SV wave AVAZ data for fracture indicator: Synthetic example

Huaizhen Chen* and Kristopher A. Innanen

ABSTRACT

Shear wave travel time analysis and reflection amplitude inversion can supply fracture estimation approaches established using P-wave azimuthal seismic data. Starting with rewriting SV-wave velocity as a function of normal and tangential fracture weaknesses in horizontal transversely isotropic (HTI) media, we present a new fracture indicator and express SV-wave velocities of two fractured layers across a reflection interface in terms of reflectivities of S-wave velocity and fracture indicator. Using the expressed SV-wave velocities, we derive SV-SV wave reflection coefficient based on a simplified version of Zoeppritz equations' solution, and we also present SV-SV wave anisotropic elastic impedance (EI) and its normalized form. Based on the derived reflection coefficient and anisotropic EI, we propose an inversion approach of employing SV-SV wave gathers to estimate unknown parameters involving S-wave velocity of background rock, density and fracture indicator, which is implemented as: 1) the least-squares inversion for anisotropic EI of different dominant incidence angles, and 2) the estimation of fracture indicator using the first- and second-order derivatives of anisotropic EI with respect to unknown parameters. We employ noise-free and noisy synthetic seismic gathers to illustrate the robustness and stability of the inversion approach, which reveals that the proposed approach may be reserved as a valuable tool for identifying fractures using SV-SV wave seismic gathers.

INTRODUCTION

Shear wave data are acquired and processed for estimating the presence of fractures in carbonate, tight sand and shale reservoirs. Shear wave splitting is a phenomenon that shear wave splits into two waves (i.e. SV and SH waves) in the case of propagating in fractured rocks, which has been successfully employed to predict fracture symmetry (Teng, 1999; Liu and Martinez, 2014). Shear waves are almost unaffected by fluids in pores and fractures (Mavko et al., 2009), and inversion of shear-wave reflection amplitude and traveltime anisotropy may provide more valuable information for the detection of natural fractures.

Differences between SV- and SH-wave traveltime, which are dependent on SV- and SH-wave velocities, are directly utilized for detecting underground fractured layers. Tsvankin and Thomsen (1995) show SV- and SH-wave velocities in terms of anisotropic parameters (ϵ, δ and γ) given by Thomsen (1986) and implement traveltime inversion using the quartic Taylor series. Combining crack model given by Hudson (1980) and linear-slip model proposed by Schoenberg and Sayers (1995), Bakulin et al. (2000) present relationships between Thomsen anisotropic parameters and fracture weaknesses (δ_{N} and δ_{T}). Berryman (2008) derives exact SV- and SH-wave velocities for transversely isotropic (TI) media with a vertical and horizontal axis (VTI and HTI media) as a function of incidence and azimuthal

*School of Ocean and Earth Science, Tongji University, Shanghai, China; and CREWES Project, University of Calgary, Calgary, Alberta, Canada. Email: huaizhen.chen@ucalgary.ca

angles. Using relationships between Thomsen anisotropic parameters and fracture weaknesses, the incidence- and azimuthal-angle-dependent SV-wave velocity can be related to fracture weaknesses directly.

Reflection amplitude variation with incidence angle (AVA) is observed in pre-stacked seismic angle gathers. Zoeppritz equations are solved to obtain exact and approximate reflection coefficients of different seismic waves (e.g. P-to-P, P-to-SV, SV-to-SV, SV-to-P). Under the assumption of isotropic media, Aki and Richards (2002) present approximate reflection coefficients of different seismic waves in terms of reflectivities of seismic wave velocities. In anisotropic media, extended Zoeppritz equations are proposed by Schoenberg and Protazio (1992) to obtain exact solutions of seismic wave reflection coefficients. In the case of VTI and HTI media, Rüger (1996) derives P-to-P, P-to-SV, SV-to-SV wave approximate reflection coefficients in terms of reflectivities of isotropic background rock elastic properties and perturbations in Thomsen anisotropic parameters. In addition to AVA, reflection amplitude variation with azimuthal angle is also observed (AVAZ) in HTI media.

A rock with a set of vertically aligned fractures is assumed to be a HTI medium (Bakulin et al., 2000; Berryman, 2009). P-to-P wave AVAZ datasets have been widely employed to estimate fracture related parameters (e.g. Thomsen anisotropic parameters, fracture weaknesses) under the assumption of HTI media, which leads to the prediction of natural fractures in hydrocarbon reservoirs (Downton and Benjamin, 2010; Downton and Roure, 2015; Chen et al., 2018a). Using simplified and approximate reflection coefficient, Martins (2006) presents an anisotropic elastic impedance of P-to-P wave ($\mathrm{EI}_{\mathrm{PP}}$). Based on fluid substitution model proposed for anisotropic media (Mavko et al., 2009), Chen and Zhang (2017) implement inversion of azimuthal seismic datasets to estimate dry fracture weaknesses and fluid bulk modulus. Although some studies on using P-to-P wave to predict fracture parameters have been carried out, shear wave surveys and processing make it possible to improve the accuracy of fracture parameter estimation because of shear waves being mainly affected by fractures and not sensitive to fluids.

Joint inversion is implemented to employ P-to-P and P-to-SV wave data to estimate Thomsen parameters or fracture weaknesses in anisotropic media. Grechka et al. (1999, 2005) present an approach of joint inversion of P and PS wave velocities and reflection data to estimate anisotropic parameters in orthorhombic media. Chang et al. (2017) use a physical model to analyze converted shear wave AVAZ in a reservoir with vertically aligned fractures. Chen et al. (2018b) establised an inversion approach and workflow of employing PP- and PSV-wave AVAZ data to estimate fracture compliances in HTI media. However, SV-to-P and SV-to-SV wave AVAZ are not sufficiently employed in fractured reservoirs.

In the present study, we aim to establish an inversion approach and workflow of employing SV-wave velocity variation with incidence and azimuthal angles (VVAZ) and SV-to-SV wave AVAZ to estimate fracture indicator. We first re-express the incidence- and azimuth-dependent SV-wave velocity in HTI media as a function of fracture weaknesses, from which we present a new fracture indicator. Using approximate solutions of Zoeppritz equations and the re-expressed SV-wave velocity, we derive a linearized reflection coefficient of SV-to-SV wave in terms of reflectivities of isotropic background S-wave velocity, density and fracture indicator, and we also present an anisotropic elastic impedance of SV-to-SV wave

($\mathrm{EI_{SS}}$). Based on the derived reflection coefficient and anisotropic $\mathrm{EI_{SS}}$, we propose an inversion approach of employing SV-to-SV wave datasets to estimate fracture indicator, which is implemented as: 1) the inversion for $\mathrm{EI_{SS}}$, and 2) the estimation of fracture indicator using the inverted $\mathrm{EI_{SS}}$. Synthetic seismic angle gathers of different signal-to-noise ratios (SNR) are utilized to verify the robustness and stability of the proposed inversion approach.

THEORY AND METHOD

We re-express SV-wave velocity as a function of fracture weaknesses and write incidence- and azimuthal-angle-dependent SV-wave velocities of upper and lower fractured layers in terms of S-wave velocity reflectivity of isotropic background and perturbations in fracture weaknesses. Using the expressed SV-wave velocity, we derive SV-SV wave reflection coefficient R_{SS} and elastic impedance $\mathrm{EI_{SS}}$ as a function of fracture indicator. We establish an approach of employing azimuthal SV-SV wave amplitudes to estimate unknown parameters (S-wave velocity and density of background rock, and fracture indicator) using first- and second-order derivatives of $\mathrm{EI_{SS}}$ with respect to unknown parameters.

Re-expression of SV-wave velocity of fractured rocks

Focusing on a rock containing a set of vertical fractures with a horizontal symmetry axis, we first study the parameterization of SV-wave velocity in HTI media. Berryman (2008) presents exact and approximate expressions of SV-wave velocity in terms of Thomsen parameters (ε and δ) for the HTI media, which varies with the incidence and azimuthal angles (θ_{S} and ϕ)

$$V_{\mathrm{S}}\left(\theta_{\mathrm{S}},\phi\right) \approx \beta\left[1+\frac{C_{33}}{C_{44}}\left(\varepsilon-\delta\right)\left(\cos^2\theta_{\mathrm{S}}\sin^2\phi-\cos^4\theta_{\mathrm{S}}\sin^4\phi\right)\right], \tag{1}$$

where

$$\varepsilon=\frac{C_{11}-C_{33}}{2C_{33}},$$

$$\delta=\frac{\left(C_{13}+C_{55}\right)^2-\left(C_{33}-C_{55}\right)^2}{2C_{33}\left(C_{33}-C_{55}\right)}, \tag{2}$$

and β is S-wave velocity of the isotropic background rock. In the case of rocks with a set of vertically aligned fractures whose normals parallel to x_1 axis, stiffness parameters C_{11}, C_{13}, C_{33} and C_{55} are given by Bakulin et al. (2000) as

$$C_{11}=M\left(1-\delta_{\mathrm{N}}\right),$$

$$C_{13}=\lambda\left(1-\delta_{\mathrm{N}}\right),$$

$$C_{33}=M\left[1-(1-2g)^2\delta_{\mathrm{N}}\right],$$

$$C_{55}=\mu\left(1-\delta_{\mathrm{T}}\right), \tag{3}$$

where $M=\lambda+2\mu$, λ and μ are the Lamé constants of the isotropic background rock, $g=\mu/M$, and δ_{N} and δ_{T} are the normal and tangential fracture weaknesses that are related

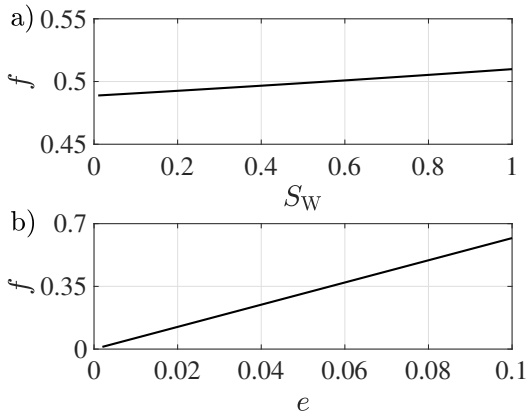

FIG. 1. a) Variation of fracture indicator f with water saturation S_{w} in the case of fracture density e of 0.08, and b) Variation of fracture indicator f with fracture density e in the case of S_{w} of 0.35. Bulk moduli of water and oil are 2.25 GPa and 1.5 GPa, S-to-P wave modulus ratio $g = 0.25$, fracture aspect ratio $\chi = 0.01$, and S-wave modulus of background rock $\mu = 25$ GPa, respectively.

to fracture properties (Appendix A). Substituting equation 3 to equation 1, we re-express the SV-wave velocity as

$$V_{\mathrm{S}}\left(\theta_{\mathrm{S}}, \phi\right) \approx \beta\left[1 + f\left(\cos^2\theta_{\mathrm{S}}\sin^2\phi - \cos^4\theta_{\mathrm{S}}\sin^4\phi\right)\right], \tag{4}$$

where $f = 2\left(\delta_{\mathrm{T}} - g\delta_{\mathrm{N}}\right)$ is a fracture indicator.

In the case that fractures are saturated with the mixture of water and oil, we model how the fracture indicator f varies with water saturation S_{W} and fracture density e, as shown in Figure 1. The fracture weaknesses δ_{N} and δ_{T} are calculated using expressions shown in Appendix A. We observe that the fracture indicator increases with fracture density, and the fracture indicator is less influenced by water saturation. Therefore, we employ f as an indicator for identifying fractured areas in underground layers.

For an interface separating two HTI media, we express the S-wave velocity of the background rock and the fracture indicator across the interface as

$$\begin{aligned}
\beta_1 &= \overline{\beta}(1 - r_\beta),\ \beta_2 = \overline{\beta}(1 + r_\beta), \\
\rho_1 &= \overline{\rho}(1 - r_\rho),\ \rho_2 = \overline{\rho}(1 + r_\rho), \\
f_1 &= \overline{f}(1 - r_f),\ f_2 = \overline{f}(1 + r_f),
\end{aligned} \tag{5}$$

where $r_\beta = \frac{\Delta\beta}{2\overline{\beta}}$, $r_\rho = \frac{\Delta\rho}{2\overline{\rho}}$, $r_f = \frac{\Delta f}{2\overline{f}}$, $\overline{\beta}$, $\overline{\rho}$, and $\overline{f}$ are average results of isotropic background rock S-wave velocity, density and fracture indicator of the upper and lower layers, respectively.

Substituting equation 5 to equation 4, we derive SV-wave velocities of the upper and lower fractured layers as

$$\begin{aligned}
V_{\mathrm{S1}}\left(\theta_{\mathrm{S1}}, \phi\right) &\approx \overline{\beta}(1 - r_\beta)\left[1 + \overline{f}(1 - r_f)\left(\cos^2\theta_{\mathrm{S1}}\sin^2\phi - \cos^4\theta_{\mathrm{S1}}\sin^4\phi\right)\right] \\
&\approx \overline{\beta}(1 - r_\beta) + \overline{\beta}\,\overline{f}(1 - r_\beta - r_f)\left(\cos^2\theta_{\mathrm{S1}}\sin^2\phi - \cos^4\theta_{\mathrm{S1}}\sin^4\phi\right),
\end{aligned}$$

$$\begin{aligned} V_{\mathrm{S2}}\left(\theta_{\mathrm{S2}},\phi\right) &\approx \overline{\beta}(1+r_\beta)\left[1+\overline{f}(1+r_f)\left(\cos^2\theta_{\mathrm{S2}}\sin^2\phi-\cos^4\theta_{\mathrm{S2}}\sin^4\phi\right)\right] \\ &\approx \overline{\beta}(1+r_\beta)+\overline{\beta}\,\overline{f}(1+r_\beta+r_f)\left(\cos^2\theta_{\mathrm{S2}}\sin^2\phi-\cos^4\theta_{\mathrm{S2}}\sin^4\phi\right), \end{aligned} \tag{6}$$

in which we neglect the term proportional to $r_\beta r_f$.

Azimuthal reflection coefficient and elastic impedance of SV-SV wave in HTI media

Zoeppritz equations are solved to obtain reflection and transmission coefficients of plane waves (Aki and Richards, 2002). Ikelle and Amundsen (2018) present explicit expressions of reflection coefficients using P- and S-wave velocities for a reflection interface separating two isotropic media. SV-SV wave reflection coefficient R_{SS} is given by (Ikelle and Amundsen, 2018)

$$R_{\mathrm{SS}} = -\frac{c_2 d_1 + c_4 d_3}{d_1 d_2 + d_4 d_3}, \tag{7}$$

where

$$d_1 = 2K^2\Delta G\left(\sqrt{V_{\mathrm{P1}}^{-2}-K^2}-\sqrt{V_{\mathrm{P2}}^{-2}-K^2}\right)+\left(\rho_1\sqrt{V_{\mathrm{P2}}^{-2}-K^2}+\rho_2\sqrt{V_{\mathrm{P1}}^{-2}-K^2}\right),$$

$$d_2 = 2K^2\Delta G\left(\sqrt{V_{\mathrm{S1}}^{-2}-K^2}-\sqrt{V_{\mathrm{S2}}^{-2}-K^2}\right)+\left(\rho_1\sqrt{V_{\mathrm{S2}}^{-2}-K^2}+\rho_2\sqrt{V_{\mathrm{S1}}^{-2}-K^2}\right),$$

$$d_3 = K\left[2\Delta G\left(\sqrt{V_{\mathrm{P1}}^{-2}-K^2}\sqrt{V_{\mathrm{S2}}^{-2}-K^2}+K^2\right)-\Delta\rho\right],$$

$$d_4 = K\left[2\Delta G\left(\sqrt{V_{\mathrm{P2}}^{-2}-K^2}\sqrt{V_{\mathrm{S1}}^{-2}-K^2}+K^2\right)-\Delta\rho\right],$$

$$c_2 = -\left[2K^2\Delta G\left(\sqrt{V_{\mathrm{S1}}^{-2}-K^2}+\sqrt{V_{\mathrm{S2}}^{-2}-K^2}\right)-\left(\rho_1\sqrt{V_{\mathrm{S2}}^{-2}-K^2}-\rho_2\sqrt{V_{\mathrm{S1}}^{-2}-K^2}\right)\right],$$

$$c_4 = -K\left[2\Delta G\left(\sqrt{V_{\mathrm{P2}}^{-2}-K^2}\sqrt{V_{\mathrm{S1}}^{-2}-K^2}-K^2\right)+\Delta\rho\right], \tag{8}$$

where $\Delta G = \rho_2(V_{\mathrm{S2}})^2 - \rho_1(V_{\mathrm{S1}})^2$ is the difference between shear moduli of upper and lower fractured layers, V_{P1} and V_{P2} are P-wave velocities of the upper and lower fractured layers, $K = \frac{\sin\theta_{\mathrm{S1}}}{V_{\mathrm{S1}}} = \frac{\sin\theta_{\mathrm{S2}}}{V_{\mathrm{S2}}}$ is the approximate ray parameter in anisotropic media, in which θ_{P1} and θ_{S1} are angles of reflected P and S waves in the upper layer, and θ_{P2} and θ_{S2} are angles of transmitted P and S waves in the lower layer, respectively.

Chen et al. (2018a) conclude that in the case of low fracture density and small fracture weaknesses the approximate form of Snell's law is applicable in anisotropic media. In this study, we focus on deriving the reflection coefficient of SV-SV wave (R_{SS}) in the case of the normal and tangential fracture weaknesses being small (i.e. $\delta_{\mathrm{N}} \ll 1$ and $\delta_{\mathrm{T}} \ll 1$).

Under the assumption of small changes in elastic properties and fracture weaknesses across the reflection interface, we neglect the term proportional to $\Delta G\Delta\rho$, $(\Delta G)^2$, and $(\Delta\rho)^2$ in equation 7 to further simplify reflection coefficients of SV-SV wave as

$$R_{\mathrm{SS}}\left(\overline{\theta}_{\mathrm{S}},\phi\right)\approx-\frac{c_2}{d_2}\approx a_\rho\left(\overline{\theta}_{\mathrm{S}}\right)r_\rho+a_\beta\left(\overline{\theta}_{\mathrm{S}}\right)r_\beta+a_f\left(\overline{\theta}_{\mathrm{S}},\phi\right)\Delta f, \tag{9}$$

where

$$\begin{aligned}
a_\rho\left(\overline{\theta}_{\mathrm{S}}\right)&=1+4\sin^2\overline{\theta}_{\mathrm{S}},\\
a_\beta\left(\overline{\theta}_{\mathrm{S}}\right)&=\frac{1}{2}\sec^2\overline{\theta}_{\mathrm{S}}+\frac{1}{2}+8\sin^2\overline{\theta}_{\mathrm{S}},\\
a_f\left(\overline{\theta}_{\mathrm{S}},\phi\right)&=\frac{1}{2}\cos^2\overline{\theta}_{\mathrm{S}}\sin^2\phi\left(8\sin^2\overline{\theta}_{\mathrm{S}}+1\right)\left(1-\cos^2\overline{\theta}_{\mathrm{S}}\sin^2\phi\right),
\end{aligned} \tag{10}$$

and where $\overline{\theta}_{\mathrm{S}}$ is the average of S-wave incidence and transmission angles (i.e. $\overline{\theta}_{\mathrm{S}}=\frac{\theta_{\mathrm{S1}}+\theta_{\mathrm{S2}}}{2}$).

Martins (2006) presents an anisotropic elastic impedance (EI) formula of PP wave in terms of weakly anisotropic parameters; and Chen et al. (2018a) propose azimuthal reflection coefficient of PP wave as a function of dry fracture weaknesses and fluid bulk modulus, which leads to the establishment of two-step inversion approach of employing azimuthal PP-wave seismic datasets to estimate indicators of fractures and fluids. Under the assumption that $R_{\mathrm{SS}}\approx\Delta\mathrm{EI}_{\mathrm{SS}}/(2\mathrm{EI}_{\mathrm{SS}})$, we further propose azimuthal anisotropic EI of SV-SV wave ($\mathrm{EI}_{\mathrm{SS}}$) as

$$\mathrm{EI}_{\mathrm{SS}}\left(\overline{\theta}_{\mathrm{S}},\phi\right)=\rho^{a_\rho\left(\overline{\theta}_{\mathrm{S}}\right)}\,\beta^{a_\beta\left(\overline{\theta}_{\mathrm{S}}\right)}\,\exp\left[2a_f\left(\overline{\theta}_{\mathrm{S}},\phi\right)f\right]. \tag{11}$$

Following Whitcombe (2002), we propose a partially normalized SV-SV wave EI, in which we solely normalize the term related to S-wave velocity and density

$$\mathrm{EI}_{\mathrm{SS}}\left(\overline{\theta}_{\mathrm{S}},\phi\right)=\beta_0\rho_0\left(\frac{\rho}{\rho_0}\right)^{a_\rho\left(\overline{\theta}_{\mathrm{S}}\right)}\left(\frac{\beta}{\beta_0}\right)^{a_\beta\left(\overline{\theta}_{\mathrm{S}}\right)}\exp\left[2a_f\left(\overline{\theta}_{\mathrm{S}},\phi\right)f\right], \tag{12}$$

where β_0 and ρ_0 are constant values of S-wave velocity and density, respectively.

We next calculate SV-SV wave reflection coefficient for a model of an interface separating two fractured layers. Table 1 shows S-wave velocity β, density ρ, and fracture weaknesses δ_{N} and δ_{T} of the model.

Table 1. S-wave velocity, density and fracture weaknesses of two fractured layers

	β (m/s)	ρ (g/cm^3)	δ_{N}	δ_{T}
Layer 1	2500	2.25	0.02	0.01
Layer 2	3000	2.3	0.6	0.35

We show variations of R_{SS} with the incidence angle $\overline{\theta}_{\mathrm{S}}$ and azimuth ϕ in Figure 2. Figure 2a) shows how R_{SS} varies with $\overline{\theta}_{\mathrm{S}}$ in the case of ϕ of 0° and 45°, and Figure 2b)

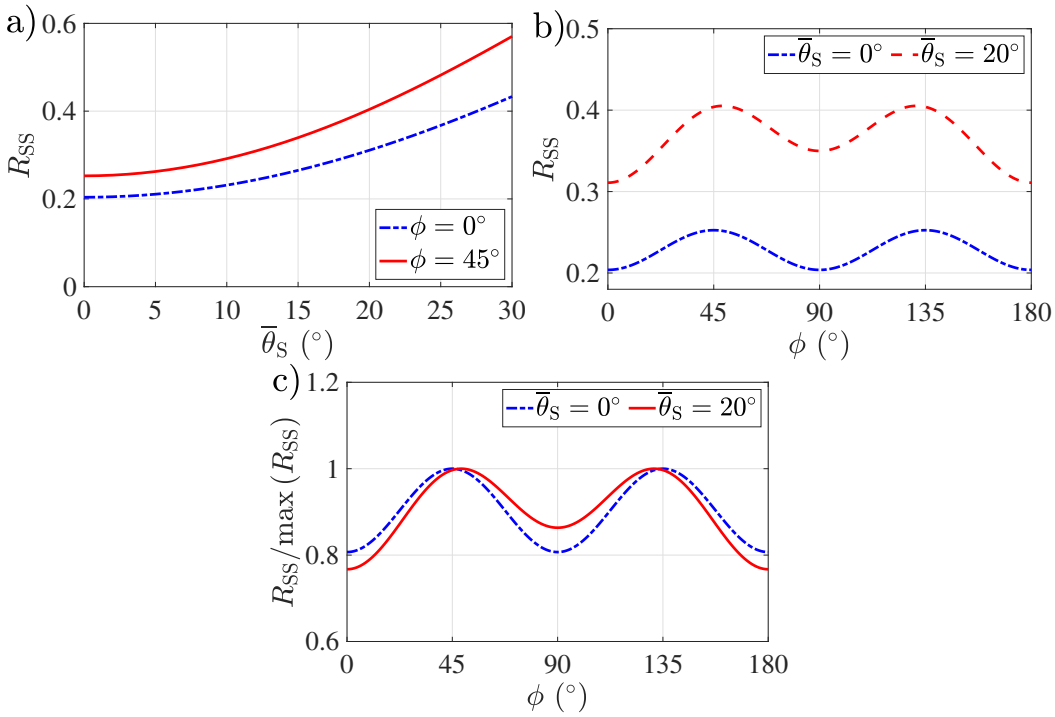

FIG. 2. a) Variation of R_{SS} with azimuthal angle ϕ; b) Variation of R_{SS} with the incidence angle θ_S; and c) Normalized R_{SS} computed as $\frac{R_{SS}}{\max(R_{SS})}$ variation with azimuthal angle ϕ.

shows the variation of R_{SS} with ϕ in the case of $\overline{\theta}_S$ of $0°$ and $20°$. In Figure 2a), we observe the difference between $R_{SS}\left(\overline{\theta}_S, \phi = 0°\right)$ and $R_{SS}\left(\overline{\theta}_S, \phi = 45°\right)$ increases with $\overline{\theta}_S$, and in Figure 2b), we intuitively observe that in the case of a large incident angle ($\overline{\theta}_{SS}$ of $20°$), the variation of R_{SS} with ϕ becomes obvious. We next compare the variation of normalized R_{SS} with ϕ in the case of $\overline{\theta}_S$ of $0°$ and $20°$ in Figure 2c), and we observe that the normalized $R_{SS}\left(\overline{\theta}_S = 0°, \phi\right)$ is close to the normalized $R_{SS}\left(\overline{\theta}_S = 20°, \phi\right)$.

We conclude that different from P-to-P wave reflection coefficient variation with azimuth that becomes more obvious at the large incidence angle discussed by Rüger (1996) and Chang et al. (2017), SV-to-SV wave reflection coefficient variation with azimuth is observable at small and middle angles. It implies that to invert for fracture indicator f using SV-SV reflection amplitudes, datasets of small- and middle-offset may already meet the requirements.

Inversion of azimuthal SS-wave amplitudes for fracture indicator

Based on different parameterized EI, a two-step inversion approach of using pre-stacked seismic data to estimate unknown parameters from pre-stacked seismic datasets, which is mainly implemented as: 1) employing pre-stacked PP-wave data to estimate PP-wave EI datasets of different incidence angles; and 2) using the EI datasets to estimate unknown parameters (e.g. P- and S-wave velocities or moduli) using a Bayesian framework (Whitcombe et al., 2002; Martins, 2006; Zong et al., 2013; Chen et al., 2018a). In the present study, we employ pre-stacked azimuthal SV-SV wave datasets to implement a new two-step inversion for estimating the unknown parameter vector $\mathbf{m}$ involving S-wave velocity,

density and fracture indicator.

We first employ an iterative damped least-squares method to estimate SV-SV wave EI, and the input datasets are partially incidence-angle-stacked SV-SV wave seismic amplitudes of different azimuthal angles. In the case of n reflection interfaces and l incidence angles, the forward modeling of SV-SV wave gathers is implemented using S-wave wavelet and SV-SV wave EI

$$\mathbf{s} = \mathbf{A}\,\mathbf{e}, \tag{13}$$

where $\mathbf{A} = \mathbf{WD}$, $\mathbf{D}$ is a difference matrix, $\mathbf{W}$ is vector of S-wave wavelet, and $\mathbf{s}$ and $\mathbf{e}$ are vectors of seismic gather and logarithmic EI (LEI), which are given by

$$\mathbf{s} = \begin{bmatrix} s_1\left(\overline{\theta}_{\mathrm{S}j}, \phi_k\right) \\ s_2\left(\overline{\theta}_{\mathrm{S}j}, \phi_k\right) \\ \vdots \\ s_i\left(\overline{\theta}_{\mathrm{S}j}, \phi_k\right) \\ \vdots \\ s_n\left(\overline{\theta}_{\mathrm{S}j}, \phi_k\right) \end{bmatrix}_{n\times 1},$$

$$\mathbf{W} = \begin{bmatrix} w_1 & 0 & \dots & \dots & 0 \\ w_2 & w_1 & 0 & \dots & 0 \\ \vdots & w_2 & \ddots & \ddots & \vdots \\ \vdots & \vdots & \ddots & \ddots & 0 \\ w_n & \dots & \dots & w_2 & w_1 \end{bmatrix}_{n\times n},$$

$$\mathbf{D} = \begin{bmatrix} -\frac{1}{2} & \frac{1}{2} & & & & \\ & -\frac{1}{2} & \frac{1}{2} & & & \\ & & \ddots & \ddots & & \\ & & & & -\frac{1}{2} & \frac{1}{2} \end{bmatrix}_{n\times(n+1)},$$

$$\mathbf{e} = \begin{bmatrix} \mathrm{LEI}^1_{\mathrm{SS}}\left(\overline{\theta}_{\mathrm{S}j}, \phi_k\right) \\ \mathrm{LEI}^2_{\mathrm{SS}}\left(\overline{\theta}_{\mathrm{S}j}, \phi_k\right) \\ \vdots \\ \mathrm{LEI}^i_{\mathrm{SS}}\left(\overline{\theta}_{\mathrm{S}j}, \phi_k\right) \\ \vdots \\ \mathrm{LEI}^{n+1}_{\mathrm{SS}}\left(\overline{\theta}_{\mathrm{S}j}, \phi_k\right) \end{bmatrix}_{(n+1)\times 1}, \tag{14}$$

where $s_i\left(\overline{\theta}_{\mathrm{S}j}, \phi_k\right)$ is ith sample of seismic gather at incidence angle $\overline{\theta}_{\mathrm{S}j}$ and azimuth ϕ_k, $w_1, ..., w_n$ are samples of S-wave wavelet, and $\mathrm{LEI}^i_{\mathrm{SS}}\left(\overline{\theta}_{\mathrm{S}j}, \phi_k\right)$ is ith sample of logarithmic EI at incidence angle $\overline{\theta}_{\mathrm{S}j}$ and azimuth ϕ_k, respectively.

We employ an iterative least-squares method to implement the deconvolution for estimating $\mathrm{EI}_{\mathrm{SS}}$, which is implemented as

$$\mathbf{e}_{K+1} = \mathbf{e}_K + \left(\mathbf{A}^T\mathbf{A} + \sigma\mathbf{I}\right)^{-1}\mathbf{A}^T\left(\mathbf{s} - \mathbf{A}\,\mathbf{e}_K\right), \tag{15}$$

where the subscripts represent the number of iteration, $\mathbf{A}^T$ is transposed matrix of $\mathbf{A}$, $\mathbf{I}$ is the identity matrix, and σ is a damping factor that is related to signal-to-noise ratio (SNR) of input seismic datasets.

The traditional operation in the second-step inversion is to input the logarithmic EI datasets to implement a Bayesian maximum likelihood inversion to estimate the unknown parameter vector in the case of assuming a linear relationship between vectors of model and input data. Based on the derived equation of $\mathrm{EI}_{\mathrm{SS}}$, we express a nonlinear relationship between the vector of input EI datasets and the vector of unknown parameters as

$$\mathbf{d} = \mathbf{G}(\mathbf{m}), \tag{16}$$

where $\mathbf{d}$ is actually the inversion result of $\mathbf{e}$ in equation 15, $\mathbf{G}$ is the nonlinear operator that is related to angles of incidence and azimuth, and

$$\mathbf{m} = \begin{bmatrix} \boldsymbol{\beta} \\ \boldsymbol{\rho} \\ \boldsymbol{f} \end{bmatrix}_{3(n+1)\times 1}, \tag{17}$$

where

$$\boldsymbol{\beta} = \begin{bmatrix} \beta_1 \\ \vdots \\ \beta_i \\ \vdots \\ \beta_{n+1} \end{bmatrix}_{(n+1)\times 1},$$

$$\boldsymbol{\rho} = \begin{bmatrix} \rho_1 \\ \vdots \\ \rho_i \\ \vdots \\ \rho_{n+1} \end{bmatrix}_{(n+1)\times 1},$$

$$\boldsymbol{f} = \begin{bmatrix} f_1 \\ \vdots \\ f_i \\ \vdots \\ f_{n+1} \end{bmatrix}_{(n+1)\times 1}, \tag{18}$$

where β_i, ρ_i and f_i represent ith samples of S-wave velocity, density and fracture indicator, respectively. Using $\mathbf{d}_{\mathrm{obs}}$ as the vector of input EI datasets and $\mathbf{d}_{\mathrm{mod}}$ as the vector of EI calculated using a model $\mathbf{m}_{\mathrm{mod}}$, we express the L2-norm of misfit as

$$\mathbf{F} = \frac{1}{2}\left(\mathbf{d}_{\mathrm{obs}} - \mathbf{d}_{\mathrm{mod}}\right)^T \left(\mathbf{d}_{\mathrm{obs}} - \mathbf{d}_{\mathrm{mod}}\right). \tag{19}$$

Starting at an initial model $\mathbf{m}_i = [\boldsymbol{\beta}_i \;\; \boldsymbol{\rho}_i \;\; \mathbf{f}_i]^T$ we need to find an optimum model that leads to the minimum of the L2-norm of misfit in an iterative way

$$\mathbf{m}_{i+1} = \mathbf{m}_i + \Delta\mathbf{m}_i, \tag{20}$$

where $\Delta\mathbf{m}_i$ is the perturbation in the unknown parameter vector. The Taylor series of L2-norm of misfit is given by

$$\mathbf{F}\left(\mathbf{m}_i + \Delta\mathbf{m}_i\right) \approx \mathbf{F}\left(\mathbf{m}_i\right) + \left.\frac{\partial \mathbf{F}}{\partial \mathbf{m}}\right|_{\mathbf{m}=\mathbf{m}_i} \Delta\mathbf{m}_i + \frac{1}{2}\left.\frac{\partial^2 \mathbf{F}}{\partial \mathbf{m}^2}\right|_{\mathbf{m}=\mathbf{m}_i} \left(\Delta\mathbf{m}_i\right)^2, \tag{21}$$

and setting the derivative of $\mathbf{F}\left(\mathbf{m}_i + \Delta\mathbf{m}_i\right)$ with respect to $\Delta\mathbf{m}_i$ zero, we obtain the solution of $\Delta\mathbf{m}_i$ as

$$\Delta\mathbf{m}_i = -\left(\left.\frac{\partial^2 \mathbf{F}}{\partial \mathbf{m}^2}\right|_{\mathbf{m}=\mathbf{m}_i}\right)^{-1} \left.\frac{\partial \mathbf{F}}{\partial \mathbf{m}}\right|_{\mathbf{m}=\mathbf{m}_i}, \tag{22}$$

where

$$\begin{aligned}
\left.\frac{\partial \mathbf{F}}{\partial \mathbf{m}}\right|_{\mathbf{m}=\mathbf{m}_i} &= \left.\frac{\partial \mathbf{d}_{\mathrm{mod}}}{\partial \mathbf{m}}\right|_{\mathbf{m}=\mathbf{m}_i} \cdot \left(\mathbf{d}_{\mathrm{mod}}|_{\mathbf{m}=\mathbf{m}_i} - \mathbf{d}_{\mathrm{obs}}\right), \\
\left.\frac{\partial^2 \mathbf{F}}{\partial \mathbf{m}^2}\right|_{\mathbf{m}=\mathbf{m}_i} &= \left.\frac{\partial^2 \mathbf{d}_{\mathrm{mod}}}{\partial \mathbf{m}^2}\right|_{\mathbf{m}=\mathbf{m}_i} \cdot \left(\mathbf{d}_{\mathrm{mod}}|_{\mathbf{m}=\mathbf{m}_i} - \mathbf{d}_{\mathrm{obs}}\right) + diag\left(\left.\frac{\partial \mathbf{d}_{\mathrm{mod}}}{\partial \mathbf{m}}\right|_{\mathbf{m}=\mathbf{m}_i}\right)^2.
\end{aligned} \tag{23}$$

The first- and second-order derivatives of $\mathbf{d}_{\mathrm{mod}}$ with respect to $\mathbf{m}$ are calculated based on the derived expression of SV-SV wave EI as

$$\left.\frac{\partial \mathbf{d}_{\mathrm{mod}}}{\partial \mathbf{m}}\right|_{\mathbf{m}=\mathbf{m}_i} = \begin{bmatrix} \left.\frac{\partial \mathrm{EI}_{\mathrm{SS}}}{\partial \boldsymbol{\beta}}\right|_{\boldsymbol{\beta}=\boldsymbol{\beta}_i} \\ \left.\frac{\partial \mathrm{EI}_{\mathrm{SS}}}{\partial \boldsymbol{\rho}}\right|_{\boldsymbol{\rho}=\boldsymbol{\rho}_i} \\ \left.\frac{\partial \mathrm{EI}_{\mathrm{SS}}}{\partial \mathbf{f}}\right|_{\mathbf{f}=\mathbf{f}_i} \end{bmatrix}_{3(n+1)\times 1},$$

$$\left.\frac{\partial^2 \mathbf{d}_{\mathrm{mod}}}{\partial \mathbf{m}^2}\right|_{\mathbf{m}=\mathbf{m}_i} \approx \begin{bmatrix} \left.\frac{\partial^2 \mathrm{EI}_{\mathrm{SS}}}{\partial \boldsymbol{\beta}^2}\right|_{\boldsymbol{\beta}=\boldsymbol{\beta}_i} & & \\ & \left.\frac{\partial^2 \mathrm{EI}_{\mathrm{SS}}}{\partial \boldsymbol{\rho}^2}\right|_{\boldsymbol{\rho}=\boldsymbol{\rho}_i} & \\ & & \left.\frac{\partial^2 \mathrm{EI}_{\mathrm{SS}}}{\partial \mathbf{f}^2}\right|_{\mathbf{f}=\mathbf{f}_i} \end{bmatrix}_{3(n+1)\times 3(n+1)}. \tag{24}$$

We emphasize that different from the procedure used in full waveform inversion (FWI) presented by Köhn (2011), we directly compute first- and second-order derivatives, $\frac{\partial \mathbf{d}_{\mathrm{mod}}}{\partial \mathbf{m}}$ and $\frac{\partial^2 \mathbf{d}_{\mathrm{mod}}}{\partial \mathbf{m}^2}$, based on the derived SV-SV wave elastic impedance. The novelty of this study is that we employ involve the first- and second-order derivatives of EI with respect to unknown parameters into the inversion, which is different from the conventional Bayesian maximum likelihood inversion based on the linearized logarithmic EI.

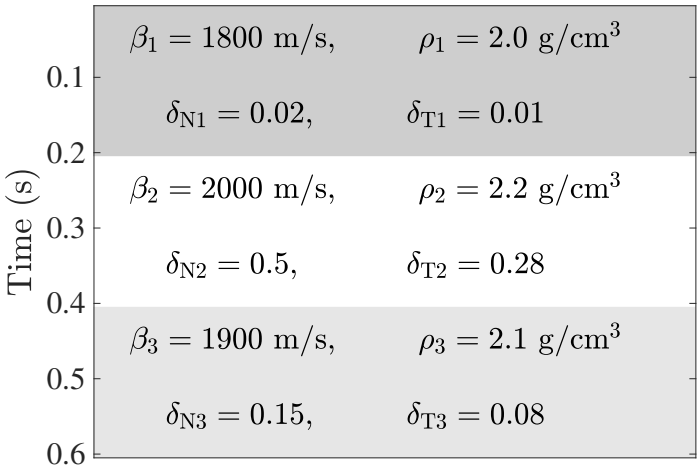

FIG. 3. A model of three fractured layers.

NUMERICAL EXAMPLES

First- and second-order derivatives of SV-SV wave EI with respect to unknown parameters

To clarify why the second-order derivatives of SV-SV wave EI with respect to unknown parameters are necessary for the inversion, we first utilize a numerical model of three fractured layers to calculate $\frac{\partial \mathbf{d}_{\rm mod}}{\partial \mathbf{m}}$ and $\frac{\partial^2 \mathbf{d}_{\rm mod}}{\partial \mathbf{m}^2}$ in the case of different incidence and azimuthal angles. S-wave velocity of the background rock, density and fracture weaknesses of a three-layer model are shown in Figure 3.

In Figure 4, we first show how the first-order derivatives of $\mathrm{EI}_{\rm SS}$ with respect to $\mathbf{m}$ vary with angles of incidence and azimuth for the second layer. We observe that the variation of $\frac{\partial \mathrm{EI}_{\rm SS}}{\partial \beta}$ with $\theta_{\rm S}$ and ϕ is similar to that of $\frac{\partial \mathrm{EI}_{\rm SS}}{\partial \rho}$, and the values of $\frac{\partial \mathrm{EI}_{\rm SS}}{\partial \beta}$ are larger than that of $\frac{\partial \mathrm{EI}_{\rm SS}}{\partial \rho}$, as shown in Figure 4d). We also see that the derivatives $\frac{\partial \mathrm{EI}_{\rm SS}}{\partial \beta}$ and $\frac{\partial \mathrm{EI}_{\rm SS}}{\partial \rho}$ are less sensitive to azimuth ϕ than $\frac{\partial \mathrm{EI}_{\rm SS}}{\partial f}$ that shows an apparent variation with ϕ especially in the case of relatively large incidence angles. It seems that we may estimate the fracture indicator f based on the calculation of first-order derivatives of different azimuthal angles; however, the first-order derivatives of $\mathrm{EI}_{\rm SS}$ are insufficient for the estimation of β and ρ.

In Figure 5, we plot the variation of the second-order derivatives of $\mathrm{EI}_{\rm SS}$ with respect to β, ρ and f with angles of incidence and azimuth. We observe that the variation of $\frac{\partial^2 \mathrm{EI}_{\rm SS}}{\partial \beta^2}$ with θ is more apparent than that of $\frac{\partial^2 \mathrm{EI}_{\rm SS}}{\partial \rho^2}$. Hence, combination of first- and second-order derivatives of $\mathrm{EI}_{\rm SS}$ with respect to the unknown parameter vector $\mathbf{m}$ may help to improve the accuracy of inversion for β, ρ, f using azimuthal seismic amplitude data.

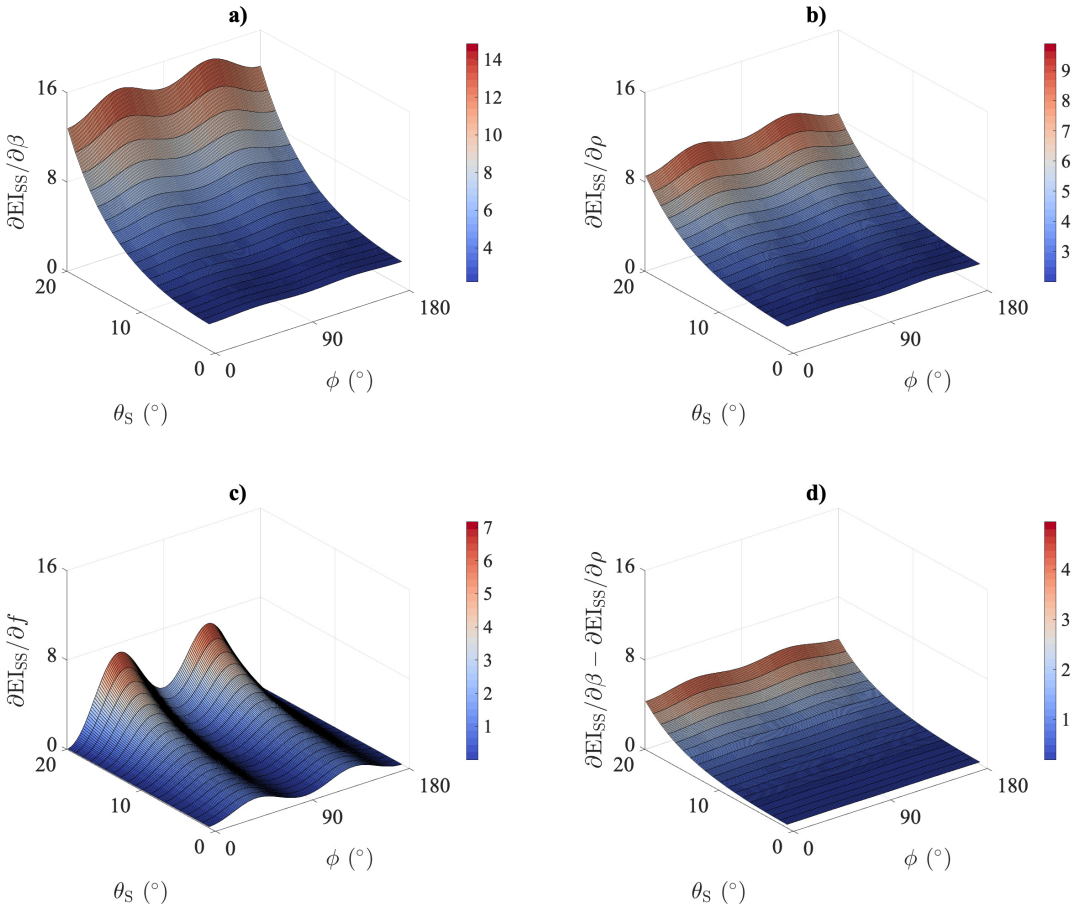

FIG. 4. The first-order derivatives of SV-SV wave EI with respect to unknown parameters. a) $\frac{\partial \mathrm{EI_{SS}}}{\partial \beta}$, b) $\frac{\partial \mathrm{EI_{SS}}}{\partial \rho}$, c) $\frac{\partial \mathrm{EI_{SS}}}{\partial f}$, and d) $\frac{\partial \mathrm{EI_{SS}}}{\partial \beta} - \frac{\partial \mathrm{EI_{SS}}}{\partial \rho}$.

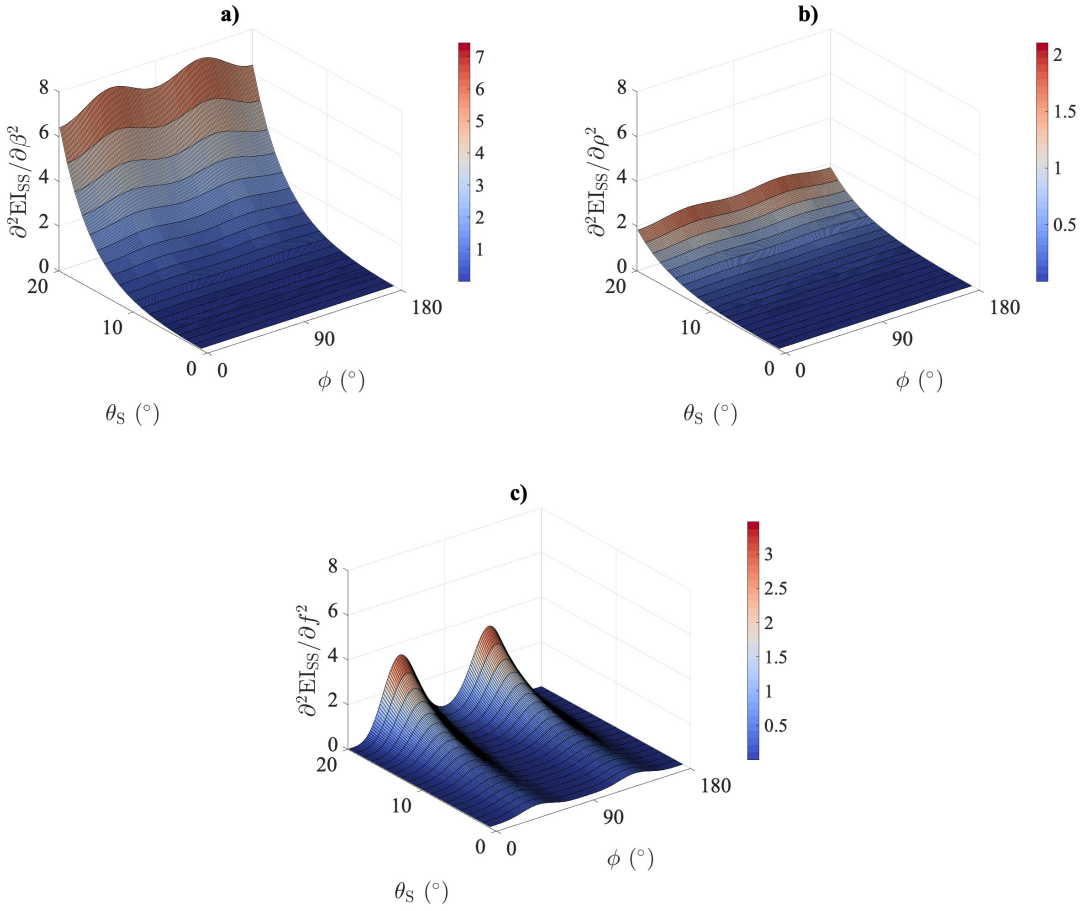

FIG. 5. The second-order derivatives of SV-SV wave EI with respect to unknown parameters. a) $\frac{\partial^2 \mathrm{EI}_{\mathrm{SS}}}{\partial \beta^2}$, b) $\frac{\partial^2 \mathrm{EI}_{\mathrm{SS}}}{\partial \rho^2}$, and c) $\frac{\partial^2 \mathrm{EI}_{\mathrm{SS}}}{\partial f^2}$.

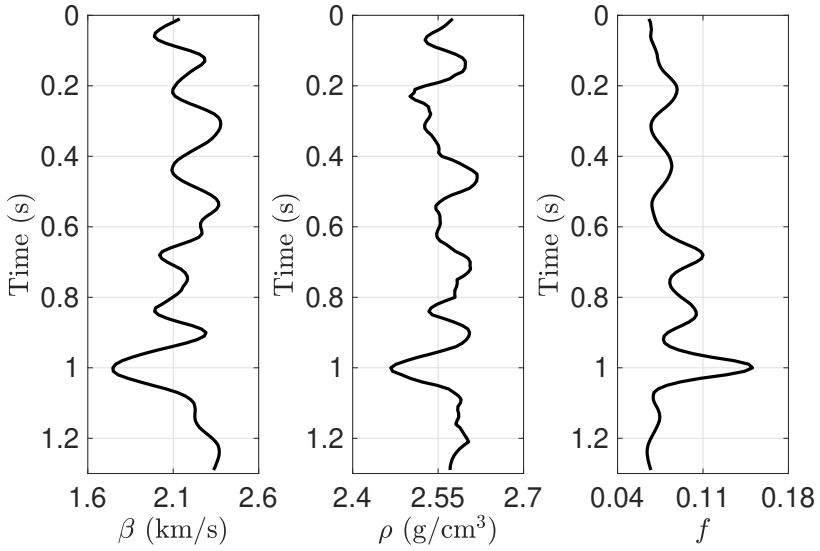

FIG. 6. Curves of S-wave velocity β, density ρ and fracture indicator f.

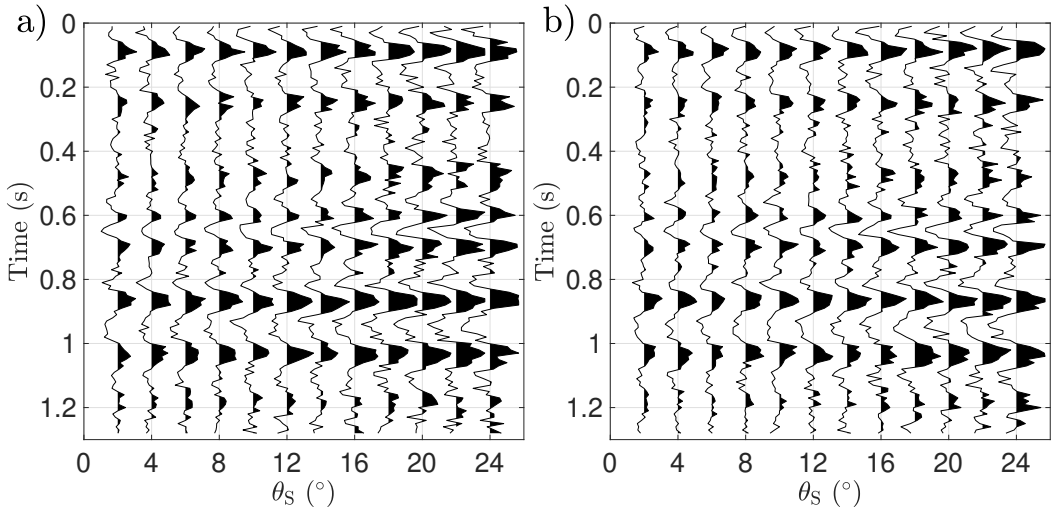

FIG. 7. Synthetic seismic gathers. a) $\phi_1 = 5°$, and b) $\phi_2 = 45°$.

Inversion for S-wave velocity, density and fracture indicator

A well log model

We proceed to the inversion for unknown parameters involving S-wave velocity β, density ρ and fracture indicator f using a well log model. S-wave velocity, density and fracture indicator are shown in Figure 6.

Given a 25Hz Ricker wavelet, we generate SV-SV wave angle gathers of azimuthal angles $\phi_1 = 5°$ and $\phi_2 = 45°$ using equation 13, and we add Gaussian random noise to the generated gathers to obtain noisy seismic angle gathers of signal-to-noise ratio (SNR) of 2, as plotted in Figure 7.

As outlined in the previous section, we first implement the inversion for EI using an it-

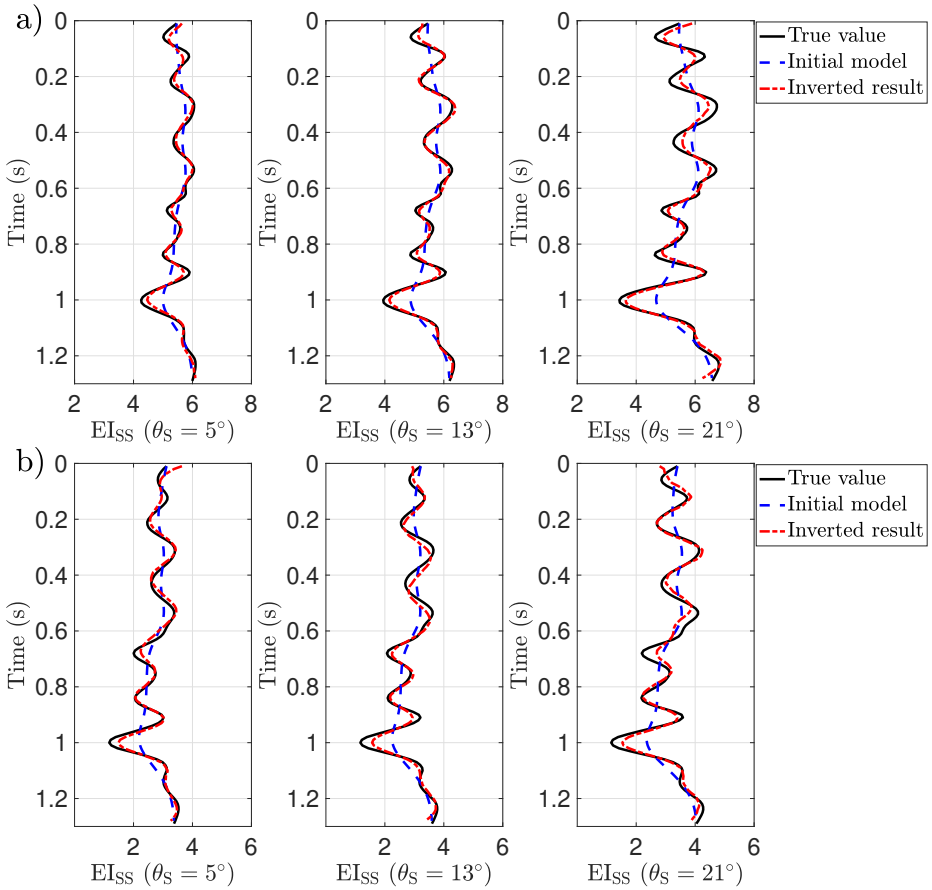

FIG. 8. Comparisons between inversion results and true values of $\mathrm{EI_{SS}}$. a) $\phi_1 = 5°$, and b) $\phi_2 = 45°$. Dashed curve represents the initial model, which is a smoothed version of true value.

erative least-squares method, and the input datasets are stacked seismic gathers that are obtained using the generated noisy seismic gathers of different incidence angle ranges (small angle range $2° - 8°$, middle angle range $10° - 16°$, and large angle range $18° - 24°$).

Comparisons between inverted results of $\mathrm{EI_{SS}}$ and the corresponding true values are shown in Figure 8. We observe there is a good match between the inversion results and true values of $\mathrm{EI_{SS}}$, which illustrates that the inversion results of $\mathrm{EI_{SS}}$ can be employed as the input datasets for the estimation of S-wave velocity β, density ρ and fracture indicator f.

Using the inverted $\mathrm{EI_{SS}}$, we first compute the first- and second-order derivatives of elastic impedance with respect to β, ρ and f, as shown in Figure 9. Using the calculated first- and second-order derivatives of $\mathrm{EI_{SS}}$ with respect to β, ρ and f, we next compute the perturbation in the unknown parameter vector $\Delta\mathbf{m}$. The final inversion results of β, ρ and f are the average values of that calculated using $\Delta\mathbf{m}$ and the initial values $\mathbf{m}_0$.

In Figure 10, we show comparisons between final inversion results and true values of β, ρ and f. We observe the inversion results of β, ρ and f can match the true values, which illustrates that we may obtain reliable estimated results of S-wave velocity, density and fracture indicator using the proposed inversion approach in the case of employing synthetic seismic gathers of SNR of 2. It reveals that the proposed inversion approach can generate

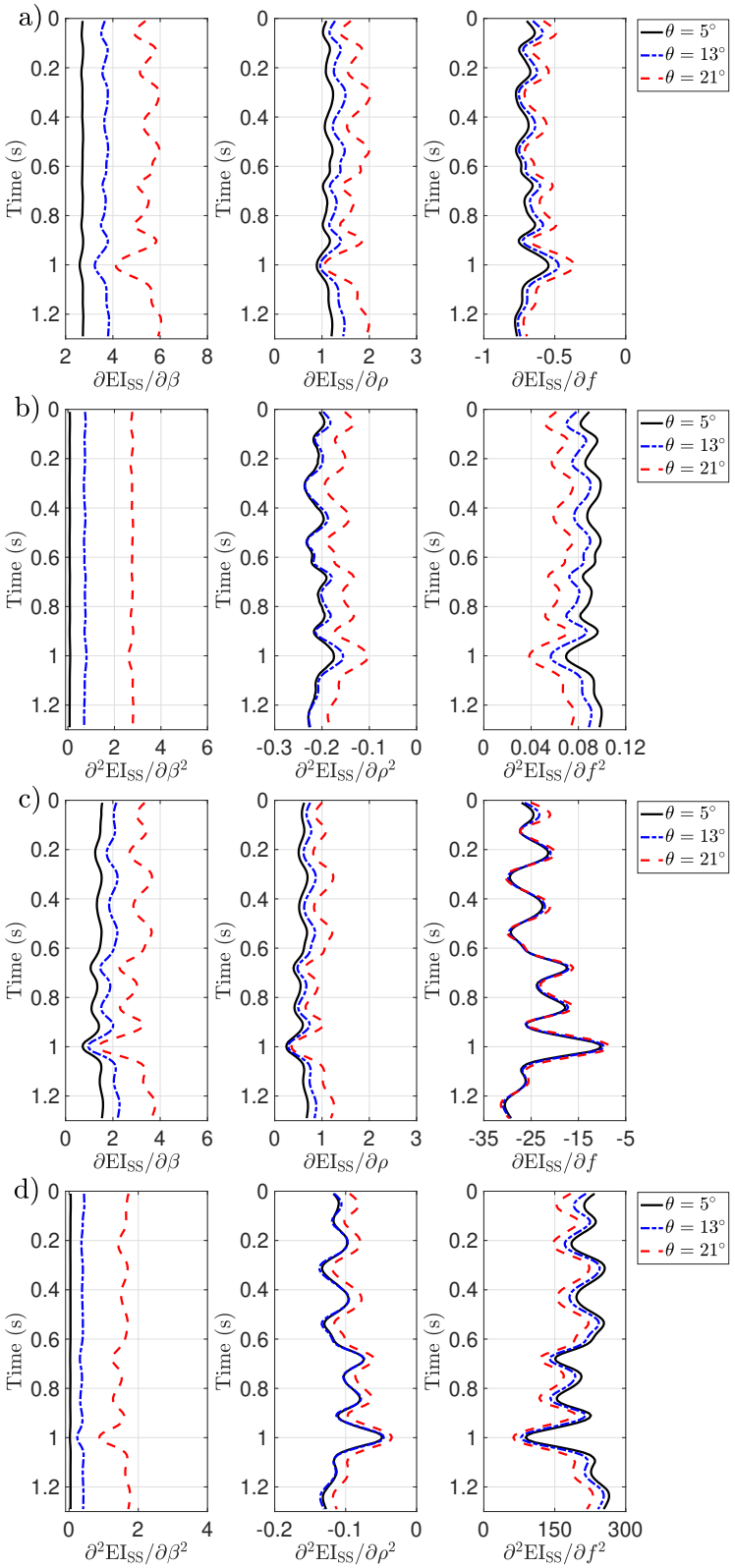

FIG. 9. a) and b) First- and second-order derivatives of $\mathrm{EI_{SS}}$ with respect to β, ρ and f at $\phi_1 = 5°$; c) and d) First- and second-order derivatives of $\mathrm{EI_{SS}}$ with respect to β, ρ and f at $\phi_2 = 45°$;

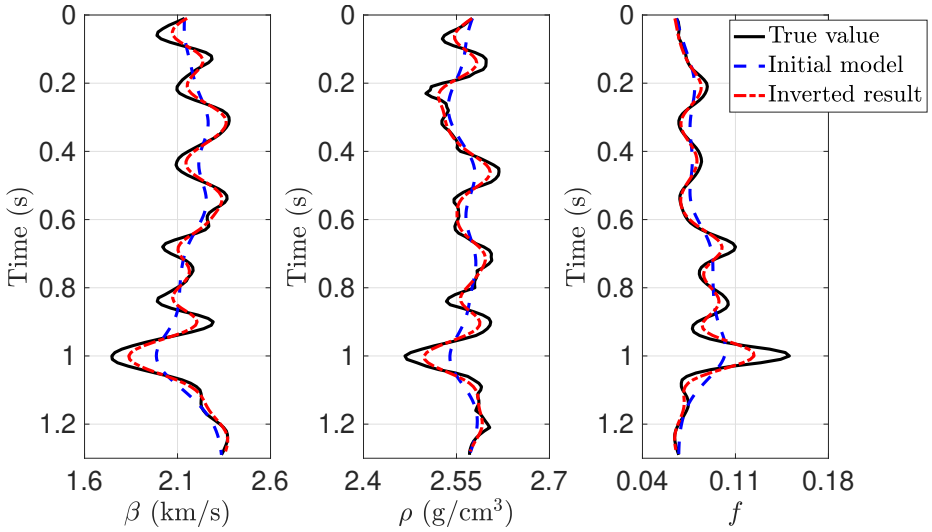

FIG. 10. Comparisons between inversion results and true values of S-wave velocity β, density ρ and fracture indicator f. Dashed curve represents the initial model, which is a smoothed version of true value.

reliable and stable indicators that are valuable for identifying fractured areas.

CONCLUSION

Based on the linear-slip model, we first re-express the incidence- and azimuthal-angle-dependent SV-wave velocity as a function of fracture indicator that is related to fracture parameters (i.e. fracture density and infilling modulus). Combining the re-expressed SV-wave velocities of upper and lower fractured layers, we derive an approximate SV-SV wave reflection coefficient and elastic impedance ($\mathrm{EI_{SS}}$) in terms of density, the background S-wave velocity and fracture indicator using the solution of Zoeppritz equations. Using the derived reflection coefficient and elastic impedance, we establish an inversion approach of employing SV-SV wave seismic gathers to estimate unknown parameters involving the background S-wave velocity, density and fracture indicator.

Numerical modeling of SV-SV AVAZ reveals that SV-SV wave reflection coefficient variation with azimuth angle is more obvious at the small and middle incidence angles, and to estimate fracture indicators using SV-SV AVAZ data, reflection amplitudes of small- and middle-offset may meet the requirements. Using the established inversion approach, we implement the inversion for S-wave velocity, density and fracture indicator using the first- and second-order derivatives of SV-SV wave $\mathrm{EI_{SS}}$ with respect to unknown parameters. Applying the proposed inversion approach to noise-free and noisy synthetic seismic gathers, we may obtain reliable results of S-wave velocity, density and fracture indicator even in the case of signal-to-noise ratio (SNR) of 2, which verifies the robustness of the inversion approach. We conclude that the proposed inversion approach can be preserved as an valuable tool of employing SV-SV wave seismic gathers to estimate indicators for fracture identification.

ACKNOWLEDGMENTS

We thank the sponsors of CREWES for continued support. This work was funded by CREWES industrial sponsors, and NSERC (Natural Science and Engineering Research Council of Canada) through the grant CRDPJ 461179-13. This work was also funded by Shanghai Sailing Program and was supported by the Fundamental Research Funds for the Central Universities.

REFERENCES

Aki, K., and Richards, P. G., 2002, Quantitative seismology: University Science Books.

Bakulin, A., Grechka, V., and Tsvankin, I., 2000, Estimation of fracture parameters from reflection seismic data—Part I: HTI model due to a single fracture set: Geophysics, **65**, No. 6, 1788–1802.

Berryman, J. G., 2008, Exact seismic velocities for transversely isotropic media and extended thomsen formulas for stronger anisotropies: Geophysics, **73**, No. 1, D1–D10.

Berryman, J. G., 2009, Aligned vertical fractures, HTI reservoir symmetry and thomsen seismic anisotropy parameters for polar media: Geophysical Prospecting, **57**, 193–208.

Chang, C.-H., Chang, Y.-F., and Tseng, P.-Y., 2017, Azimuthal variation of converted-wave amplitude in a reservoirwith vertically aligned fractures - a physical model study: Geophysical Prospecting, **65**, 221–228.

Chen, H., Ji, Y., and Innanen, K. A., 2018a, Estimation of modified fluid factor and dry fracture weaknesses using azimuthal elastic impedance: Geophysics, **83**, No. 1, WA73–WA88.

Chen, H., and Zhang, G., 2017, Estimation of dry fracture weakness, porosity, and fluid modulus using observable seismic reflection data in a gas-bearing reservoir: Geophysics, **38**, 651–678.

Chen, H., Zhang, G., Chen, T., and Yin, X., 2018b, Joint PP- and PSV-wave amplitudes versus offset and azimuth inversion for fracture compliances in horizontal transversely isotropic media: Geophysical Prospecting, **66**, 561–578.

Downton, J., and Benjamin, R., 2010, Azimuthal simultaneous elastic inversion for fracture detection, *in* SEG Technical Program Expanded Abstracts, 263–267.

Downton, J., and Roure, B., 2015, Interpreting azimuthal Fourier coefficients for anisotropic and fracture parameters: Interpretation, **3**, ST9–ST27.

Grechka, V., Pech, A., and Tsvankin, I., 2005, Parameter estimation in orthorhombic media using multicomponent wide-azimuth reflection data: Geophysics, **70**, D1–D8.

Grechka, V., Theophanist, S., and Tsvankin, I., 1999, Joint inversion of P- and PS-waves in orthorhombic media: Theory and a physical modeling study: Geophysics, **64**, 146–161.

Hudson, J., 1980, Overall properties of a cracked solid: Mathematical Proceedings of the Cambridge Philosophical Society, **88**, No. 2, 371–384.

Ikelle, L. T., and Amundsen, L., 2018, Introduction to petroleum seismology: Society of Exploration Geophysicists.

Köhn, D., 2011, Time domain 2D elastic full waveform tomography: Ph.D. thesis, University of Kiel.

Liu, E., and Martinez, A., 2014, Seismic fracture characterization, vol. 575: Elsevier.

Martins, J. L., 2006, Elastic impedance in weakly anisotropic media: Geophysics, **71**, No. 3, D73–D83.

Mavko, G., Mukerji, T., and Dvorkin, J., 2009, The rock physics handbook: Tools for seismic analysis of porous media: Cambridge university press.

Rüger, A., 1996, Reflection coefficients and azimuthal AVO analysis in anisotropic media: Ph.D. thesis, Colorado School of Mines.

Schoenberg, M., and Protazio, J., 1992, "zoeppritz" rationalized and generalized to anisotropic media: Journal of Seismic Exploration, **1**, 124–144.

Schoenberg, M., and Sayers, C. M., 1995, Seismic anisotropy of fractured rock: Geophysics, **60**, No. 1, 204–211.

Teng, L., 1999, Seismic and rock-physics characterization of fractured reservoirs.: Ph.D. thesis, Stanford University.

Thomsen, L., 1986, Weak elastic anisotropy: Geophysics, **51**, No. 10, 1954–1966.

Tsvankin, I., and Thomsen, L., 1995, Inversion of reflection traveltimes for transverse isotropy: Geophysics, **60**, No. 4, 1095–1107.

Whitcombe, D. N., 2002, Elastic impedance normalization: Geophysics, **67**, No. 1, 60–62.

Whitcombe, D. N., Connolly, P. A., Reagan, R. L., and Redshaw, T. C., 2002, Extended elastic impedance for fluid and lithology prediction: Geophysics, **67**, No. 1, 63–67.

Zong, Z., Yin, X., and Wu, G., 2013, Elastic impedance parameterization and inversion with Young's modulus and Poisson's ratio: Geophysics, **78**, No. 6, N35–N42.

APPENDIX A. EXPRESSIONS OF FRACTURE WEAKNESSES δ_{N} AND δ_{T}

Expressions of fracture weaknesses δ_{N} and δ_{T} are proposed relating the penny-shaped crack model given by Hudson (1980) and the linear slip model given by Schoenberg and Sayers (1995). In the case of fluid-saturated fractures, the normal and tangential fracture weaknesses are expressed as

$$\begin{aligned} \delta_{\mathrm{N}} &= \frac{4e}{3g\left(1-g\right)\left[1+\frac{1}{\pi(1-g)}\frac{K_{\mathrm{f}}}{\mu\chi}\right]}, \\ \delta_{\mathrm{T}} &= \frac{16e}{3(3-2g)}, \end{aligned} \tag{A.1}$$

where K_{f} is the effect bulk modulus of fluids in fractures, e is fracture density, and χ is fracture aspect ratio, respectively. In the case of fluids being a mixture of water and oil, the effective bulk modulus K_{f} is computed as

$$K_{\mathrm{f}} = 1/\left[S_{\mathrm{W}}/K_{\mathrm{W}} + \left(1-S_{\mathrm{W}}\right)/K_{O}\right], \tag{A.2}$$

where S_{W} is water saturation, K_{W} and K_{O} are bulk moduli of water and oil, respectively.